23rd ABCM International Congress of Mechanical Engineering
December 6-11, 2015, Rio de Janeiro, RJ, Brazil

NUMERICAL INVESTIGATION OF FORCED CONVECTION OF NON-NEWTONIAN FLUIDS ACROSS A SQUARE CYLINDER

Daniel Dall'Onder dos Santos
Luís Gustavo Souza Machado
Federal University of Uberlândia, Av. João Naves de Ávila 2121, Uberlândia, MG, 38408-100, Brazil
dallonder@femec.ufu.br
luisgustavo19@gmail.com

Abstract. *Several fluids found in industrial processes exhibit non Newtonian behavior. In some applications, these materials are subjected to heat transfer by forced convection. The main goal of this work is to perform numerical simulations of non-isothermal two-dimensional steady state laminar flows of non Newtonian fluids through a planar channel obstructed by a square cylinder. The mechanical model is defined by the mass, momentum and energy balance equations coupled to non Newtonian constitutive models for pseudoplastic and viscoplastic fluids. This modeling is approximated by a stabilized multi-field Galerkin finite element methodology, having as primal variables the extra-stress, velocity, pressure and temperature fields. In this way, the compatibility conditions between the extra-stress-velocity and pressure-velocity finite element subspaces are violated, allowing the use of equal-order finite element interpolations. In the performed numerical simulations, the fluid rheological parameters, namely the jump number, the power-law coefficient, the flow intensity and the non-dimensional density, as well as the Prandtl number, are varied in order to evaluate their influence on the heat transfer through the geometry.*

Keywords: *forced convection heat transfer, multi-field mechanical modeling, Galerkin least-squares method, non-Newtonian fluids*

1. INTRODUCTION

The fluids found in nature, in its vast majority, have non-Newtonian characteristics. Among them, there is a class of liquids that appear to have a yield stress. In early studies, given the limited strain rate range of measurement of the first rheometers, it was believed that below a certain stress level (the yield stress) the viscosity of this fluids could be assumed infinite, and below this stress the material could be seen as a rigid body (Barnes, 1999). With the advance of the experimental apparatus employed in these measurements, it was observed that these materials, once defined as rigid bodies, have a high, but finite, viscosity, even below the apparent yield stress. Therefore, different constitutive models began to emerge on the literature to model and understand the stress-strain relation of viscoplastic materials when in different flow conditions.

Different engineering applications deal with viscoplastic fluid flows, as processes in the food industry (production of yoghurt, chocolate and cream cheese), chemical and petrochemical industries (petroleum, polymer solutions, adhesives and rubbers) and natural processes (e.g. flow of blood through the circulatory system). Some of these processes include heat exchange between the fluid and its container or with the pipes the fluid is flowing through. And, as viscosity varies with the strain rate, the flow dynamics is also highly dependent on the rheological properties, what has an important effect over convection heat transfer (da Silva *et al.*, 2014).

This study aims to simulate two-dimensional flows of non-Newtonian fluids through a channel with a heated obstacle in its center. Some works found in the literature are also concerned about similar flow conditions and heat transfer on non-Newtonian fluids. In Paliwal *et al.* (2013), two-dimensional flows of power-law fluids flowing over a cylinder of square section are simulated using a finite difference numerical code. The shear-thinning, shear-thickening, Reynlods and Peclet number effects on the flow were evaluated for a fixed channel blockage ratio. The heat transfer was investigated using two different boundary conditions over the cylinder surface: heat flux and constant temperature. Patnana *et al.* (2019) studied numerically the flow of power-law fluids over and unconfined circular cylinder to understand the dependence of the drag and lift coefficients on the Reynolds number and on the power-law index. Rao *et al.* (2011) observed the behavior of a power-law fluid flowing over a prism of square cross section to evaluate the values of the Reynolds number which denotes the flow separation for shear-thinning and shear-thickening fluids. They also investigated the dependence on both the Reynolds and Prandtl numbers for the heat transfer rate. In Aboueian-Jahromi *et al.* (2011), the authors also studied a two-dimensional flow and heat transfer over a confined square cylinder, however the cylinder was inclined. The effects of the inclination angle and the power-law index on the pumping power and Nusselt number were investigated considering a fixed blockage ratio and Prandtl number. Siqueira *et al.* (2013) investigated numerically flows of power-law fluids over a cylinder of square section in several configurations. The authors varied the power-law index and the prism blocking ratio for a fixed Reynolds number, ranging the Prandtl number. The simulations were performed on an open source software, enabling the implementation of different routines, such as non-Newtonian ones.

The mechanical model employed in this work to simulate the convection heat transfer on viscoplastic fluids flowing over a heated square cylinder is based on the mass, momentum and energy balance equations coupled to the SMD constitutive equation – proposed by de Souza Mendes and Dutra (2004). The set of equations is approximated by the Galerkin-Least Squares finite element methodolody. This formulation does not need to satisfy the Ladyzhenskaya-Babuška-Brezzi condition. The stability enhancement is provided by the addition of mesh-dependent terms in the flow governing equations on a least squares form, affording, as well, the use of an equal order combination of linear finite element interpolations for the velocity, pressure, stress and temperature fields. This numerical methodology allows the investigation of how the rheological properties affects the capability of the fluid to exchange heat. Therefore, the jump number, the power-law coefficient, the flow intensity, the non-dimensional density and the Prandtl number are varied and a comparison on the Nusselt number is performed.

2. THE MECHANICAL MODEL

The relevant equations for a multi-field boundary value problem accounting for non-isothermal and incompressible flows of viscoplastic fluids may be formed by coupling the mass, momentum and energy balance equations with the SMD constitutive equation, proposed by de Souza Mendes and Dutra (2004). This model has the same qualitative behavior observed for most viscoplastic liquids of interest: a high-viscosity plateau at low shear rates, followed by a sharp drop of the viscosity level and then a power-law region. Subjecting the system to the appropriate velocity, stress and temperature boundary conditions, it becomes

$$\begin{array}{ll}
\rho(\nabla\mathbf{u})\mathbf{u} = -\nabla p + \text{div}\,\boldsymbol{\tau} + \rho\mathbf{g}\beta(T - T_{ref}) & \text{in } \Omega \\
\boldsymbol{\tau} = 2\eta(\dot{\gamma})\mathbf{D}(\mathbf{u}) & \text{in } \Omega \\
\text{div}\,\mathbf{u} = 0 & \text{in } \Omega \\
\rho c_p(\nabla T)\mathbf{u} = \kappa\nabla^2 T + q''' & \text{in } \Omega \\
\mathbf{u} = \mathbf{u}_g & \text{over } \Gamma_g^{\mathbf{u}} \\
\boldsymbol{\tau} = \boldsymbol{\tau}_g & \text{over } \Gamma_g^{\boldsymbol{\tau}} \\
T = T_g & \text{over } \Gamma_g^{T} \\
(-p\mathbf{I} + \boldsymbol{\tau})\mathbf{n} = \mathbf{t}_h & \text{over } \Gamma_h
\end{array} \tag{1}$$

where $\mathbf{u}$ is the velocity vector, $\mathbf{D}$ the strain rate tensor, $\boldsymbol{\tau}$ is the extra-stress tensor, $\mathbf{t}_h$ is the stress vector, p the hydrostatic pressure, $\mathbf{g}$ the gravity vector, T the temperature, and T_{ref} a reference temperature; β is the volumetric thermal expansion coefficient; ρ, c_p, and κ are, respectively, the fluid density, specific heat, and thermal conductivity; η is the shear-rate-dependent viscosity, and $\dot{\gamma} = (2tr\mathbf{D}^2)^{1/2}$. $\mathbf{u}_g$, $\boldsymbol{\tau}_g$, and T_g are the imposed velocity, extra-stress, and temperature boundary conditions, respectively. It is important to mention that the buoyancy, gravitational, and heat source effects are neglected in this work, although their modeling is presented in Eq. (1).

The SMD viscosity function employed here is a modified version of the original one proposed in 2004. To avoid a non-physical behavior of the viscosity, which could tend to zero as the shear rate increases, it was added a viscosity for higher shear rate values (de Souza Mendes, 2009). The SMD model becomes

$$\eta(\dot{\gamma}) = \left(1 - exp\left(-\frac{\eta_0}{\tau_0}\dot{\gamma}\right)\right)\left(\frac{\tau_0}{\dot{\gamma}} + K\dot{\gamma}^{n-1}\right) + \eta_\infty \tag{2}$$

where τ_0 is the yield stress limit of the material, K is the consistency index, η_0 and η_∞ are, respectively, the viscosities for very low and high values of the shear rate. n is the power-law index, which controls the shear-thinning and shear-thickening of the viscosity when the material starts to flow.

2.1 Dimensionless Parameters

The dimensionless parameters employed to characterize the flows analyzed in this work are, firstly, the dimensionless flow rate or flow intensity, U^*,

$$U^* = \frac{u_c}{\dot{\gamma}_1 L_c} \tag{3}$$

where u_c is a characteristic velocity and L is a characteristic lenght, taken respectively as the channel inlet velocity and half cylinder height; $\dot{\gamma}_1$ is defined as the strain rate where the fluid actually begins to flow as a power-law one

($\dot{\gamma}_1 = (\tau_0/K)^{1/n}$) – see de Souza Mendes *et al.* (2007) or Santos *et al.* (2011) for more details. The viscosity jump when the stress is around the yield stress value is measured by the jump number J, and is written as

$$J = \frac{\eta_0 \dot{\gamma}_1}{\tau_0} - 1 \tag{4}$$

To evaluate the ratio of momentum diffusivity to thermal diffusivity it is used the Prandtl number (Pr), while the inertia effects are accounted by the non-dimensional density, given as

$$\rho^* = \frac{\rho(\dot{\gamma}_1 L_c)^2}{\tau_0} \tag{5}$$

In order to study the influence of the rheological and thermal parameters on the ability of a viscoplastic fluid to exchange heat, the Nusselt number was employed as a measure of the heat transfer between the cylinder heated surface and the fluid. The Nusselt number is defined as

$$Nu = \frac{hL}{\kappa} \tag{6}$$

where h is the convection heat transfer coefficient and L is a given lenght. To obtain an analysis of the Nusselt number as a function only of known parameters, we can write h as

$$h = \frac{q''_{surface}}{T_w - T_\infty} \tag{7}$$

where q'' is the heat transfer between the cylinder and the fluid, T_w is the wall temperature of the surface and T_∞ is the temperature of the fluid at the entrance of the channel. q'' can be defined by the Fourier's law as

$$q'' = -\kappa \left(\frac{\partial T}{\partial x_2} \right)_{surface} \tag{8}$$

Thus, combining Eq. (7) and (8), the local Nusselt number can be written as

$$Nu = -\left(\frac{\partial T}{\partial x_2} \right)_{surface} \left(\frac{L}{T_w - T_\infty} \right) = -\frac{\partial \theta^*}{\partial x_2^*} \tag{9}$$

where $\theta^* = (T - T_\infty)/(T_w - T_\infty)$ and $x_2^* = x_2/L$. To evaluate the average Nusselt number over the cylinder upper surface, Eq. (9) must be integrated over the whole surface length as

$$Nu_L = \int_0^L Nu(x_1) dx_1 \tag{10}$$

3. NUMERICAL APPROXIMATION

The Galerkin least-squares approximation for the boundary value problem defined on Eq. (1) can be written as: given the appropriate Dirichlet and Neumman boundary conditions, find the set $\boldsymbol{\tau}^h, \mathbf{u}^h, p^h, T^h \in \boldsymbol{\Sigma}^h \times \mathbf{V}^h \times P^h \times \Theta^h$ such that

$$B(\boldsymbol{\tau}^h, \mathbf{u}^h, p^h, T^h; \mathbf{S}^h, \mathbf{v}^h, q^h, \psi^h) = F(\mathbf{S}^h, \mathbf{v}^h, q^h, \psi^h) \forall (\mathbf{S}^h, \mathbf{v}^h, q^h, \psi^h) \in \boldsymbol{\Sigma}^h \times \mathbf{V}^h \times P^h \times \Theta^h \tag{11}$$

with

$$\begin{aligned}
B(\boldsymbol{\tau}^h, \mathbf{u}^h, p^h, T^h; \mathbf{S}^h, \mathbf{v}^h, q^h, \psi^h) &= \int_\Omega \rho(\nabla \mathbf{u}^h)\mathbf{u}^h \cdot \mathbf{v}^h d\Omega - \int_\Omega p^h \mathrm{div} \mathbf{v}^h d\Omega + \int_\Omega \boldsymbol{\tau}^h \cdot \mathbf{D}(\mathbf{v}^h) d\Omega \\
&+ \int_\Omega \mathrm{div}\, \mathbf{u}^h q^h d\Omega + \epsilon \int_\Omega p^h q^h d\Omega + \int_\Omega \boldsymbol{\tau}^h \cdot \mathbf{S}^h d\Omega - 2\mu \int_\Omega \mathbf{D}(\mathbf{u}^h) \cdot \mathbf{S}^h d\Omega \\
&+ \int_\Omega \rho c_p (\nabla T^h) \mathbf{u}^h\, \psi^h d\Omega + \int_\Omega \kappa \nabla T^h \cdot \nabla \psi^h d\Omega + \sum_{K \in \Omega^h} \int_\Omega \delta_{GLS}(\mathrm{Re}_K)\, \mathrm{div}\, \mathbf{v}^h\, \mathrm{div}\, \mathbf{u}^h d\Omega \\
&+ \sum_{K \in \Omega^h} \int_{\Omega_K} \alpha_{GLS}(\mathrm{Re}_K) \left(\rho(\nabla \mathbf{u}^h)\mathbf{u}^h + \nabla p^h - \mathrm{div}\, \boldsymbol{\tau}^h \right) \cdot \left(\rho(\nabla \mathbf{v}^h)\mathbf{u}^h + \nabla q^h - \mathrm{div}\, \mathbf{S}^h \right) d\Omega \\
&+ \beta_{GLS} \int_\Omega \left(\boldsymbol{\tau}^h - 2\mu \mathbf{D}(\mathbf{u}^h) \right) \cdot \left(\mathbf{S}^h - 2\mu \mathbf{D}(\mathbf{v}^h) \right) d\Omega \\
&+ \sum_{K \in \Omega^h} \int_{\Omega_K} \zeta_{GLS}(\mathrm{Pe}_K) \left(\rho c_p (\nabla T^h)\mathbf{u}^h - \kappa \nabla^2 T^h \right) \cdot \left(\rho c_p (\nabla \psi^h) \mathbf{v}^h - \kappa \nabla^2 \psi^h \right) d\Omega
\end{aligned} \tag{12}$$

and

$$
\begin{aligned}
F(\mathbf{S}^h, \mathbf{v}^h, q^h, \psi^h) = & \int_{\Omega} \rho\beta(T^h - T_{ref})\mathbf{g} \cdot \mathbf{v}^h d\Omega + \int_{\Omega} q''' \psi^h d\Omega \; + \int_{\Gamma_h} \mathbf{t}_h \cdot \mathbf{v}^h d\Gamma \\
& + \sum_{K \in \Omega^h} \int_{\Omega_K} \alpha_{GLS}(\mathrm{Re}_K) \rho\beta(T^h - T_{ref})\mathbf{g} \cdot \left(\rho(\nabla\mathbf{v}^h)\mathbf{u}^h \; + \nabla q^h \; - \mathrm{div}\,\mathbf{S}^h\right) d\Omega \\
& + \sum_{K \in \Omega^h} \int_{\Omega_K} \zeta_{GLS}(\mathrm{Pe}_K) q''' \left(\rho c_p (\nabla\psi^h)\mathbf{v}^h - \kappa\nabla^2\psi^h\right) d\Omega,
\end{aligned}
\tag{13}
$$

where $\epsilon << 1$. β_{GLS} is a positive arbitrary numerical constant set according to the error estimate introduced in Behr *et al.* (1993) – in this work it was used the value 0.5. The mesh Reynolds and Péclet numbers (Re_K and Pe_K, respectively) and the stability parameters $\alpha(\mathrm{Re}_K)$, $\delta(\mathrm{Re}_K)$, and $\zeta(\mathrm{Pe}_K)$ are defined as in Franca and Frey (1992), Franca *et al.* (1992), and Behr *et al.* (1993),

$$
\begin{aligned}
& \alpha_{GLS}(\mathrm{Re}_K) = \frac{h_K}{2\left|\mathbf{u}^h\right|_p} \xi_1(\mathrm{Re}_K) \quad , \quad \delta_{GLS}(\mathrm{Re}_K) = \lambda_d \left|\mathbf{u}^h\right|_p h_K \xi_1(\mathrm{Re}_K) \\
& \mathrm{Re}_K = \frac{\rho\, h_K \left|\mathbf{u}^h\right|_p m_k}{4\,\mu} \quad , \quad \xi_1(\mathrm{Re}_K) = \begin{cases} \mathrm{Re}_K, & \text{if } 0 \le \mathrm{Re}_K < 1 \\ 1, & \text{if } \mathrm{Re}_K \ge 1 \end{cases} \\
& \zeta_{GLS}(\mathrm{Pe}_K) = \frac{h_K}{2\left|\mathbf{u}^h\right|_p} \xi_2(\mathrm{Pe}_K) \\
& \mathrm{Pe}_K = \frac{h_K \left|\mathbf{u}^h\right|_p m_k}{2\,\kappa} \quad , \quad \xi_2(\mathrm{Pe}_K) = \begin{cases} \mathrm{Pe}_K, & \text{if } 0 \le \mathrm{Pe}_K < 1 \\ 1, & \text{if } \mathrm{Pe}_K \ge 1 \end{cases} \\
& \left|\mathbf{u}^h\right|_p = \begin{cases} \left(\sum_{i=1}^{N} \left|\mathbf{u}^h\right|^p\right)^{1/p}, & \text{if } 1 \le p < \infty \\ \max_{i=1,N} \left|u_i^h\right| \quad , & \text{if } p = \infty \end{cases} \\
& m_k = \min\{1/3, 2C_k\} \\
& C_k \sum_{K \in \Omega^h} h_K^2 \left\|\mathrm{div}\,\mathbf{S}^h\right\|_{0,K}^2 \ge \left\|\mathbf{S}^h\right\|_K^2 \quad \forall \quad \mathbf{S}^h \in \mathbf{\Sigma}^h
\end{aligned}
\tag{14}
$$

where λ_d is a positive parameter and h_K is the mesh element size.

The residual matrix problem associated with the GLS formulation defined by Eq. 11 is solved by a quasi-Newton method. At each iteration, the algorithm solves, for the incremental vector $[\mathbf{A}_{k+1}]$, the linearized system $[\mathbf{J}(\mathbf{U}_n)][\mathbf{A}_{n+1}]$ = $-[\mathbf{R}(\mathbf{U}_n)]$, with $[\mathbf{J}(\mathbf{U}_n)]$ denoting the Jacobian matrix of the residual system $[\mathbf{R}(\mathbf{U}_n)]$, for an arbitrary quasi-Newton iteration n. Next, the degree-of-freedom vector is continuously updated, $[\mathbf{U}_{n+1}] = [\mathbf{U}_n] + [\mathbf{A}_{n+1}]$, until the convergence criterion, $||[\mathbf{R}(\mathbf{U}_n)]||_\infty < 10^{-7}$, is satisfied.

4. NUMERICAL RESULTS

In this section, the multi-field Galerkin least-squares formulation defined by Eq. (11) has been employed to approximate non-isothermal viscoplastic fluid flows around a square cylinder kept between two parallel plates. Figure 1 schematically shows the geometry and the kinematic and thermal boundary conditions employed in the numerical simulations: uniform velocity profiles at the channel inlet and outlet were employed, as well as no-slip and impermeability on channel walls and on the cylinder surface, and symmetry conditions on the channel centerline ($\partial_2 u_1 = u_2 = \tau_{12} = 0$); for the energy equation, an uniform temperature profile at the channel entrance, fixed temperature at the cylinder surface and thermal insulation at the channel walls and on the symmetry centerline. The channel blockage ratio, i.e. half cylinder height ($L/2$) divided by half channel width (H) is set as 0.25. In order to guarantee fully-developed flow regions upstream and downstream of the cylinder, the mesh length upstream and downstream of the cylinder are $30L$ and $21L$, respectively. After a mesh independence procedure that compares the average Nusselt number over the cylinder's top surface for each consecutive mesh refinement, it was selected a mesh with 16,731 bilinear Lagrangian (Q1) finite elements. This mesh presented an error less then 2.9% when compared to the next more refined one, with 26,561 elements and high demands of computational effort. The unyielded and unyielded regions, respectively the black and white ones in the figures, are defined by the yield stress criterion (Mitsoulis and Zisis, 2001) – the material only flows when the magnitude of the extra stress tensor exceeds the yield stress, i.e., $|\boldsymbol{\tau}| > \tau_0$

The influence of the dimensionless parameters governing the problem on the average Nusselt number – on the cylinder upper surface – is shown in Fig. 2. The jump number, J, has very low influence in the heat exchange capability of the fluid, as pointed by the very close values presented in Fig. 2a. Given that prescribed inlet and outlet velocity profiles are

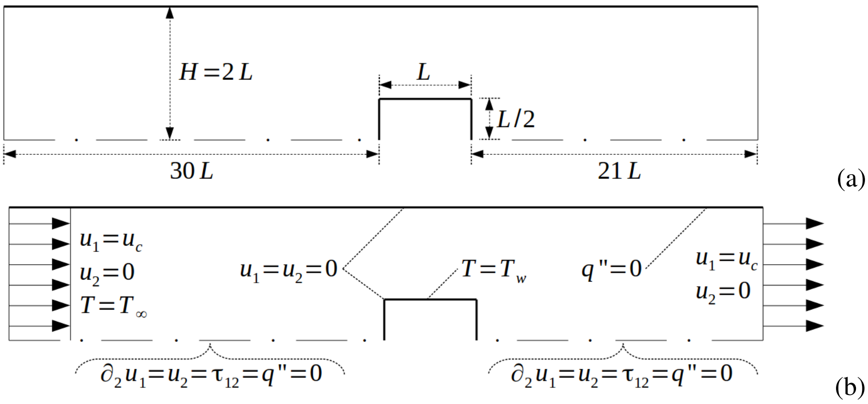

Figure 1. Planar channel with a square cylinder blocking. (a) The geometry, (b) the employed boundary conditions.

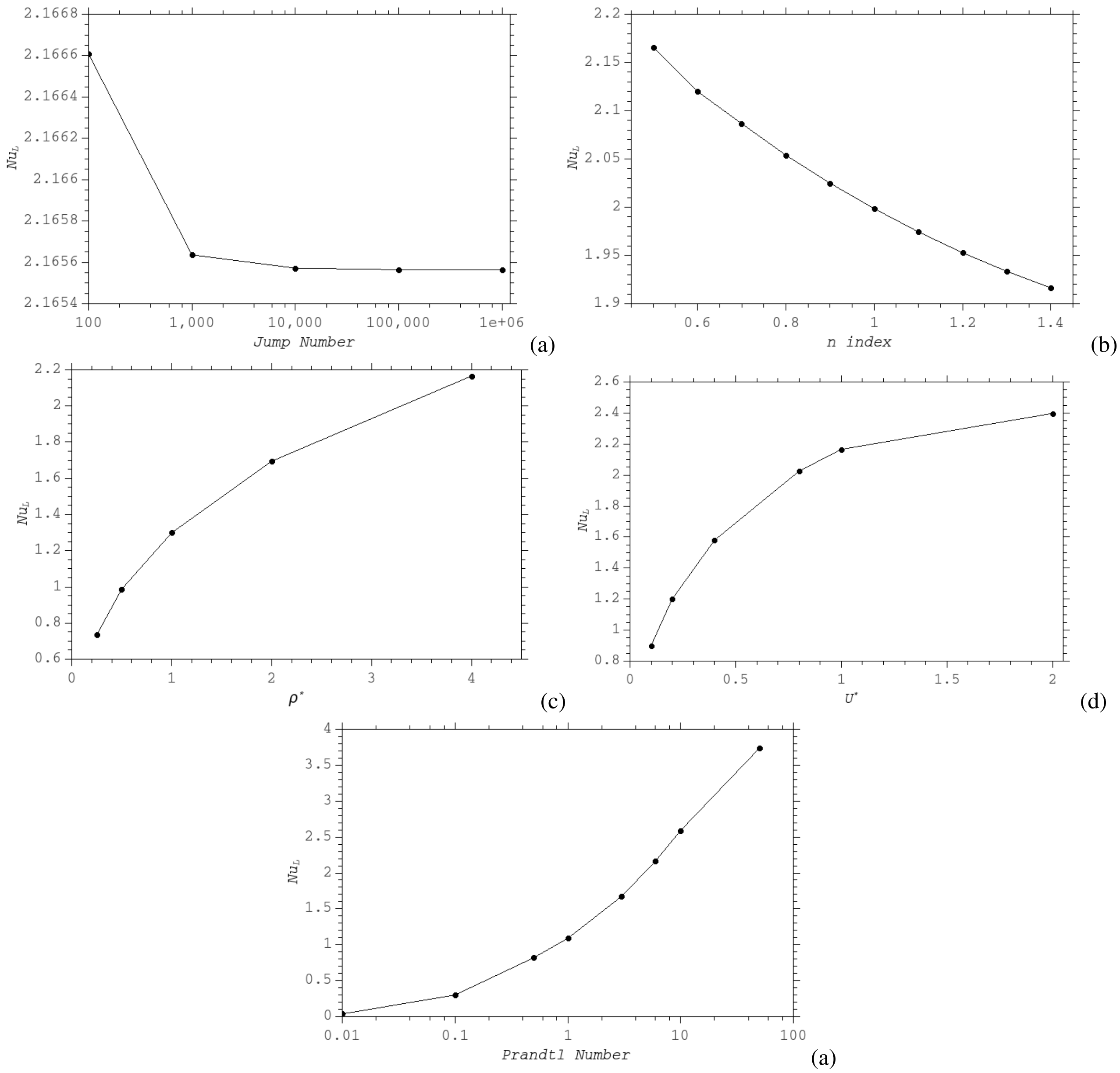

Figure 2. Effect of the dimensionless parameters on the average Nusselt number. (a) Jump number, (b) n index, (c) non-dimensional density, rho^*, (d) flow intensity, U^*, and (e) Prandtl number.

used as boundary conditions, the shear rates at the regions closer to the cylinder and to the channel walls become similar even ranging J, as shown in Fig. 3, for J=10^2 and 10^6. Therefore, the viscosity levels are identical and no considerable effect on the average Nusselt is observed.

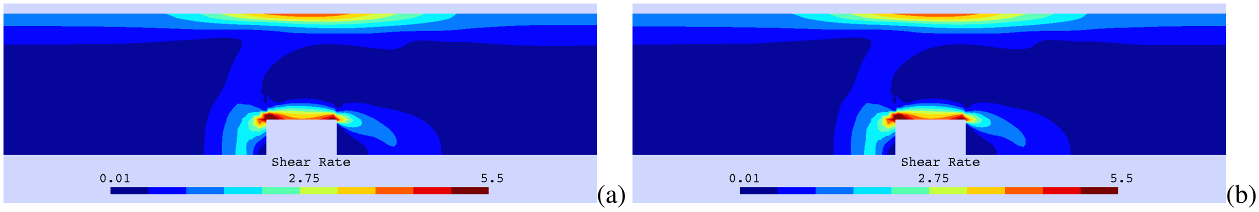

Figure 3. Effect of the jump number on the flow – shear rate for U^*=1, ρ^*=4, Pr=6, n=0.5. (a) J=10^2, and (b) J=10^6.

Figure 4 shows the flow unyielded and yielded regions (black and white, respectively) for U^*=1, ρ^*=4, Pr=6, J=10^4, n=0.5 and 1.4. As expected, as the fluid becomes thicker with the increasing of n, the unyielded regions become bigger. This viscosity increase leads to a reduction on the advective effects and less heat can be exchanged between the cylinder surface and the fluid – Fig 2b. The same trend is pointed by Siqueira *et al.* (2013) for power-law fluids.

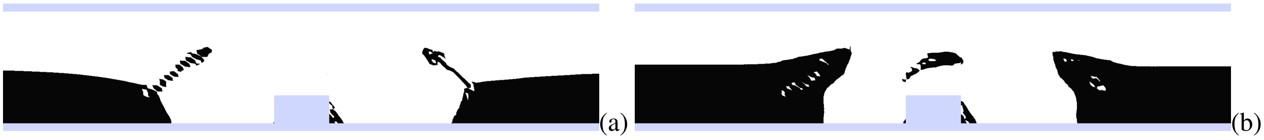

Figure 4. Effect of the n index on the flow – unyielded regions for U^*=1, ρ^*=4, Pr=6, J=10^4. (a) n=0.5, and (b) n=1.4.

The effect of inertia is illustrated on Fig. 2c and Fig. 5 for U^*=1, Pr=6, J=10^4, and n=0.5, ranging ρ^* from 0.025 to 4.0. The average Nusselt number grows with the increase of inertia. This trend comes from the augment of the advection effects in both the momentum and energy balance equations, and consequently, more energy is transfered from the cylinder to the fluid. The unyielded regions corroborate this observation: they are almost symmetrical for lower ρ^* values; increasing this parameters, this symmetry is broken, as depicted in Fig. 5b. The advantage on the use of the scaling presented in Section 2.1(de Souza Mendes, 2007) is that changes on the flow field entailed by inertia are decoupled from changes entailed by the flow intensity.

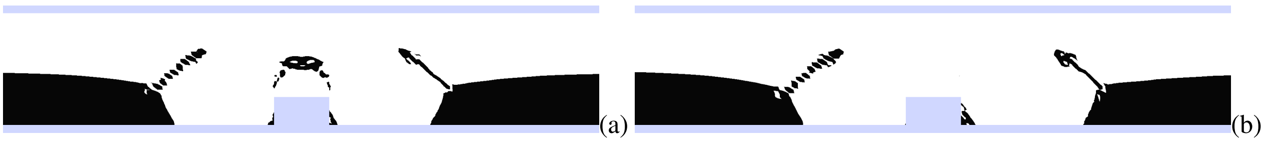

Figure 5. Effect of the non-dimensional density on the flow – unyielded regions for U^*=1, Pr=6, J=10^4, n=0.5. (a) ρ^*=0.025, and (b) ρ^*=4.0.

The flow intensity effects on the average Nusselt number and on the unyielded regions is depicted in Fig. 2d and Fig. 6, respectively, for ρ^*=4, Pr=6, n=0.5, J=10^4, ranging U^* between 0.1 and 2. Firstly, is important to stress that U^* can be seen as a measure of the fluid viscoplasticity and is related to parameters usually employed in the literature (e.g., the classical Herschel-Bulkley number – U^*=$1/\mathrm{HB}^{1/n}$. The effects observed in Fig. 6 becomes very clear when the increase of U^* is seen as a diminution on the fluid yield stress. More flow regions yields and begin to flow as a power-law fluid ($\dot{\gamma} > \dot{\gamma}_1$) favouring the convection heat transfer. Another effect, also observed by Hermany *et al.* (2013), is the lost of the fore-aft symmetry as the flow intensity increases, as different rheological states are expected for each U^*, leading to differente topology, size and location of the unyielded regions (Hermany *et al.*, 2013).

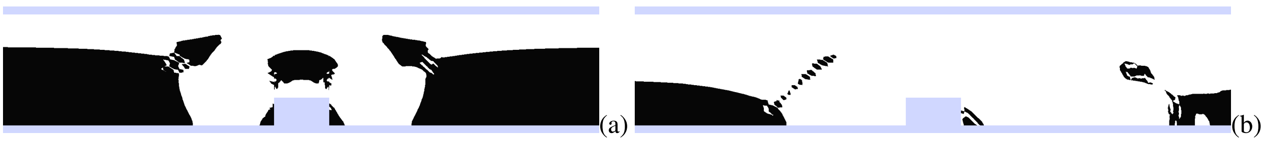

Figure 6. Effect of the flow intensity on the flow – unyielded regions for ρ^*=4, Pr=6, n=0.5, J=10^4. (a) U^*=0.1, and (b) U^*=2.

Figure 2e, Fig. 7 and Fig. 8 show the influence of the Prandtl number on the average Nusselt, unyielded regions and temperature field, respectively, for U^*=1, ρ^*=4, n=0.5, J=10^4, ranging Pr from 0.01 to 50. As mentioned before, the employed modeling does not account for buoyancy effects and changes in the viscosity with temperature. Therefore, the flow field – and consequently the unyielded regions – are not affected by the temperature field. On the other hand, the temperature field is substantially modified by the increase of the Prandtl number, as the enhance of momentum diffusivity (or diminution of thermal diffusivity) tends to carry the inlet fluid temperature information over the whole geometry – Fig. 8b.

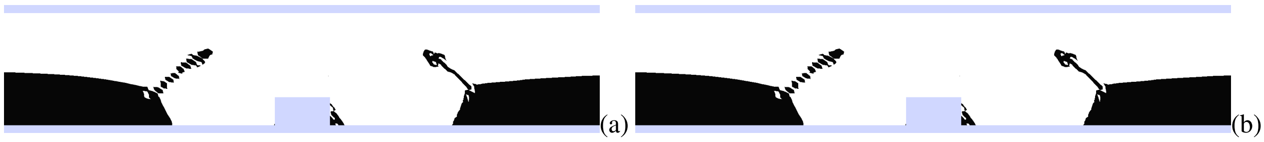

Figure 7. Effect of the Prandtl number on the flow – unyielded regions for U^*=1, ρ^*=4, n=0.5, J=10^4. (a) Pr=0.01, and (b) Pr=50.

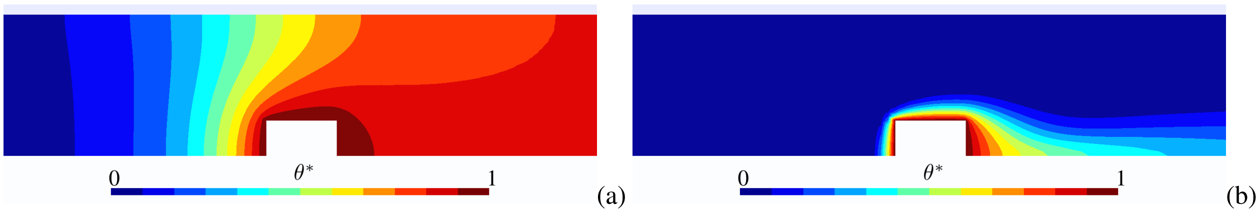

Figure 8. Effect of the Prandtl number on the temperature field for U^*=1, ρ^*=4, n=0.5, J=10^4. (a) Pr=0.1, and (b) Pr=6.

5. FINAL REMARKS

This work presents numerical results obtained for viscoplastic fluid flows through a channel with a heated obstacle in its center. The fluid properties were varied in order to evaluate the capability of heat exchange between the cylinder and the fluid. Increasing the non-dimensional density or the flow intensity have similar effects over the increase in the Nusselt number once the advection effects in both the momentum and energy balance equations are augmented. The jump number has almost no influence over the fluid exchange capability, while the power-law index increase leads to a reduction on the advective effects – what changes significantly the Nusselt number. As expected, the Prandtl number modifies substantially the temperature field, although it has no effect over the flow field due to the initial hypothesis made. It is also important to mention the stability of the finite element formulation presented in this work providing satisfactory results even for a coarse mesh.

6. ACKNOWLEDGEMENTS

The authors acknowledge FAPEMIG and the Faculty of Mechanical Engineering (FEMEC/UFU) for financial support.

7. REFERENCES

Aboueian-Jahromi, J., Nezhad, A.H. and Behzadmehr, A., 2011. "Effects of inclination angle on the steady flow and heat transfer of power-law fluids around a heated inclined square cylinder in a plane channel". *Journal of Non-Newtonian Fluid Mechanics*, Vol. 166, pp. 1406–1414.

Barnes, H.A., 1999. "The yield stress – a review or $\pi\alpha\nu\tau\alpha\ \rho\epsilon\iota$ – everything flows?" *Journal of Non-Newtonian Fluid Mechanics*, Vol. 81, pp. 133–178.

Behr, A.M., Franca, L.P. and Tezduyar, T.E., 1993. "Stabilized finite element methods for the velocity – pressure – stress formulation of incompressible flows". *Computer Methods in Applied Mechanics and Engineering*, Vol. 104, pp. 31–48.

da Silva, J.Q., Soares, E.J., Ramos, R. and Andrade, R.M., 2014. "Heat transfer to herschel-bulkley materials flowing in the entrance of tubes with an imposed wall temperature profile". *Journal of The Brazilian Society of Mechanical Sciences and Engineering*, Vol. 36, pp. 245–255. doi:10.1007/s40430-013-0078-y.

de Souza Mendes, P.R., 2007. "Dimensionless non-newtonian fluid mechanics". *Journal of Non-Newtonian Fluid Mechanics*, Vol. 147, pp. 109–116.

de Souza Mendes, P.R., 2009. "Modeling the thixotropic behavior of structured fluids". *Journal of Non-Newtonian Fluid Mechanics*, Vol. 164, pp. 66–75.

de Souza Mendes, P.R. and Dutra, E.S.S., 2004. "Viscosity function for yield-stress liquids". *Applied Rheology*, Vol. 14, pp. 296–302.

de Souza Mendes, P.R., Naccache, M.F., Varges, P.R. and Marchesini, F.H., 2007. "Flow of viscoplastic liquids through axisymmetric expansions-contractions". *Journal of Non-Newtonian Fluid Mechanics*, Vol. 142, pp. 207–217.

Franca, L.P. and Frey, S.L., 1992. "Stabilized finite element methods: Ii. the incompressible navier-stokes equations". *Computer Methods in Applied Mechanics and Engineering*, Vol. 99, pp. 209–233.

Franca, L.P., Frey, S.L. and Hughes, T.J.R., 1992. "Stabilized finite element methods: I. application to the advective-diffusive model". *Computer Methods in Applied Mechanics and Engineering*, Vol. 95, pp. 253–276.

Hermany, L., Santos, D.D., Frey, S., Naccache, M. and de Souza Mendes, P.R., 2013. "Flow of yield-stress liquids through an axisymmetric abrupt expansion-contraction". *Journal of Non-Newtonian Fluid Mechanics*, Vol. 201, pp. 1–9.

Mitsoulis, E. and Zisis, T., 2001. “Flow of bingham plastics in a lid-driven square cavity”. *Journal of Non-Newtonian Fluid Mechanics*, Vol. 101, pp. 173–180.

Paliwal, B., Sharma, A., Chhabra, R.P. and Eswaran, V., 2013. “Power law fluid flow past a square cylinder: momentum and heat transfer characteristics”. *Chemical Engineering Science*, Vol. 58, pp. 5315–5329.

Patnana, V.K., Bharti, R.P. and Chhabra, R.P., 2019. “Two-dimensional unsteady flow of power-law fluids over a cylinder”. *Chemical Engineering Science*, Vol. 64, pp. 2978–2999.

Rao, P.K., Sahu, A.K. and Chhabra, R., 2011. “Momentum and heat transfer from a square cylinder in power-law fluids”. *International Journal of Heat and Mass Transfer*, Vol. 54, pp. 390–403.

Santos, D.D., Frey, S., Naccache, M. and de Souza Mendes, P.R., 2011. “Numerical approximations for flow of viscoplastic fluids in a lid-driven cavity”. *Journal of Non-Newtonian Fluid Mechanics*, Vol. 166, pp. 667–679.

Siqueira, E.S., Zinani, F. and Indrusiak, M.L.S., 2013. “Numerical study of forced convection of a power-law fluid across a square cylinder”. In *Proceedings of the 22nd International Congress of Mechanical Engineering - COBEM 2013*. Ribeirão Preto, Brazil.

8. RESPONSIBILITY NOTICE

The authors are the only responsible for the printed material included in this paper.